IRIS AperTO

UNIVERSITÀ DEGLI STUDI DI TORINO

AperTO - Archivio Istituzionale Open Access dell'Università di Torino

Zinc oxide hollow spheres decorated with cerium dioxide. the role of morphology in the photoactivity of semiconducting oxides

This is a pre print version of the following article:

Original Citation:

Availability:

This version is available http://hdl.handle.net/2318/1886833 since 2023-01-23T16:25:07Z

Published version:

DOI:10.1088/1361-648X/ac4629

Terms of use:

Open Access

Anyone can freely access the full text of works made available as "Open Access". Works made available under a Creative Commons license can be used according to the terms and conditions of said license. Use of all other works requires consent of the right holder (author or publisher) if not exempted from copyright protection by the applicable law.

(Article begins on next page)

07 July 2024

Zinc oxide hollow spheres decorated with cerium dioxide. The role of morphology in the photoactivity of semiconducting oxides

Erik Cerrato, Mario Chiesa, Elio Giamello, Stefano Livraghi, Enrico Salvadori, Maria Cristina Paganini*

Dipartimento di Chimica, via Giuria 7, 10125 Torino

Corresponding author: mariacristina.paganini@unito.it

Zinc Oxide, hollow spheres, Cerium dioxide, photoactivity, semiconductors

Abstract

The photochemical activity of the recently proposed CeO_2-ZnO photocatalytic material active under visible light has been improved by means of significant modifications of its morphology. A polymeric templating agent (Pluronic) has been used in the synthesis obtaining a particle morphology based on hollow spheres that is better defined in the case of high template concentration. The charge separation ability and the light-induced surface electron transfer under irradiation with visible polychromatic light in various ranges of wavelenghts has been investigated by Electron Paramagnetic Resonance. The reactivity of the photogenerated holes has been monitored by the spin trapping technique in the presence of DMPO. The hollow spheres morphology achieved through the synthesis here reported leads to systems with a higher photoactivity under visible irradiation than the same system displaying the classic platelets morphology. A parallel increase of the photocatalytic activity of this novel system in pollution remediation reactions is therefore predictable.

1. Introduction

Semiconducting reducible oxides play a fundamental role as catalysts in light-driven chemical reactions aimed either to pollutant remediation or to the production of solar fuels such as hydrogen from water photosplitting. The photocatalytic performances are primarily determined by the metal oxide band gap and the corresponding oxidative and reductive potentials. However, other properties such as surface area, particle morphology and degree of crystallinity can also greatly influence the photocatalytic activity of the material.[1] As matter of fact, the efficiency of semiconducting oxides employed as photocatalyst such as ZnO, can be enhanced through the optimization of particles morphology. In particular, zinc oxide, differently from other metal oxides, can be easily synthetized in organized and hierarchical structure, increasing its interest and consideration in the photocatalytic field [2, 3].

In the recent past doping of semiconducting oxides with rare earth (RE) ions has attracted a great deal of attention due to its potential to increase the charge carriers lifetime in the solid, reducing the recombination

processes thus improving the photocatalytic performance. Most importantly, doping with RE ions also brings about a photosensitivity of the materials to frequencies in the visible range (Visible light active –VLA- systems) paving the way to a wider application of solar light in photocatalysis. Among the various oxides doped with different lanthanides ions, exciting performances were registered for Ce-doped ZnO composite materials, especially because of their activity under visible light irradiation [4-6]. The general consensus about the high photocatalytic activity under visible irradiation shown by this mixed material is however accompanied by different interpretations regarding the crystal structure and the working mechanism of this system. Despite the great discrepancy in the ionic radii of Zn^{2+}, Ce^{4+} and Ce^{3+}, having values of 0.074 nm, 0.092 nm and 0.103 nm respectively, several authors suggested the incorporation of Ce ions inside ZnO lattice. [7-10] Other authors justify the absence of a detectable CeO_2 phase postulating that Ce ions are stabilized in ZnO grain boundaries. In both cases, the presence of Ce would create discrete defect levels near the conduction band edge reducing the material band gap and hindering the recombination of the photoinduced charge carriers. [8, 11]. Alternative studies support the fact that cerium ions are not incorporated in the ZnO lattice but rather they form a separate phase (CeO_2) at the zinc oxide surface; the intimate contact between the two phases would form an active heterojunction imparting improved photocatalytic performances to the mixed system with respect to the bare oxide [12-14]. CeO_2 is considered an insulating material since the gap between the valence band, made up by 2p oxygen orbitals , and the conduction band, formed by empty 5s cerium orbitals, is almost 6 eV [15]. However, the empty cerium *4f* levels lye approximately 3 eV above the valence band edge, allowing to host photoexcited electrons. While these considerations have been largely discussed in the literature, the role of the particle morphology has received lower attention. In particular, to the best of our knowledge, only one report is present, reporting on Ce-ZnO hollow sphere particles for the photodegradation of methyl orange under UV-vis irradiation.[16]

In that study the Authors report that the degree of surface roughness and the hollow structure pattern the increasing Ce content (from 0.1 mol% to 0.5 mol%); however, no information about the role of cerium in the observed enhanced photocatalytic activity was provided.

In the present paper we will illustrate how, employing during the hydrothermal synthesis of Ce-ZnO a very simple and “clean” surfactant as the tryblock-copolymer Pluronic (P_{123}), the formation of hollow spheres is favored over that of platelets, the most typical ZnO morphology.. Interestingly, this particular hollow-sphere structure enhances the photoactivity of the systems in photoinduced processes at both the solid-gas and solid-liquid interface driven by visible light.

2. Materials and Methods

ZnO and CeO_2-ZnO Hollow Spheres Preparation

Pristine ZnO and Ce-doped ZnO containing 1% molar of cerium were prepared by hydrothermal synthesis in presence of a soft template, Pluronic (P_{123}), in different amounts. The samples were labelled ZnO-HP1 and

CZ1-HP1, pure and mixed material respectively, when the amount of P_{123} in the autoclave was 1 g, and ZnO-HP2 and CZ1-HP2 when the surfactant amount was 2 g. The bare samples were synthetized starting from the dissolution of P_{123m} in 30 mL of Ethanol and left in stirring for 4 h, in order to obtain a transparent solution. Successively, 2.2 g of $Zn(CH_3COO)_2 \bullet 2H_2O$ were added and still left in stirring for one hour; subsequently 18 mL of H_2O were added and still left in stirring for another hour. Finally, NaOH 4 M was added until a pH of 11 was reached. The suspension was sonicated for 1 h and heated at 393 K in autoclave for 5 h; the samples were collected and washed with H_2O by means centrifugation. The precipitate was dried in a stove for 12 h at 343 K. The final product was obtained calcining the precipitate firstly at 393 K for 4 h and subsequently at 773 K for 5 h. The doped samples CZ1-HP1 and CZ1-HP2, containing 1% molar of Ce, were synthetized adding the corresponding stoichiometric amount of $CeCl_3*7H_2O$ to the starting mixture.

For comparison, the same materials i.e. bare (ZnO-H) and doped (CZ1-H) zinc oxide respectively, were also prepared employing the hydrothermal method in absence of Pluronic.

Characterization Techniques

The structural phase and the crystallinity of the synthetized materials were investigated by X-ray powder diffraction (XRD). The diffraction patters were recorded with a PANalytical PW3040/60 X'Pert PRO MPD diffractometer using a copper K_α radiation source (0.154056 nm). The intensities were obtained in the 2θ range between 20° and 80°. X'Pert High-Score software was used for data handling.

The Scherrer equation has been used to evaluate the crystallite size of the existing phases:

$$D = \frac{K\lambda}{\beta cos\theta}$$

where D is the average crystallites size (in nm); K is a dimensionless shape factor often chosen as 0.9 for platelets particles, while in this case it was selected as 0.6 since the particles show spherical shape; λ is the wavelength of the radiation source, β is the full width at the half maxima and θ is the half diffraction angle.

The specific surface area measurements were carried out on a Micromeritics ASAP 2020 using the Brunauer–Emmett–Teller (BET) model on the N_2 adsorption measurement. Prior to the adsorption run, all the samples were outgassed at 573 K for 2 h.

The morphological characterisation was performed by scanning electron microscopy (SEM, secondary electron detector) and (scanning) transmission electron microscopy ((S)TEM). The images were acquired with a JEOL JEM F200 TEM (Jeol Ltd., Tokyo, Japan) which is equipped with a cold field emission source, using a TVIPS F216 2k by 2k CMOS camera (TVIPS GmbH, Gauting, Germany) and a large windowless JEOL Centurio EDX detector (100 mm2, 0.97 srad, energy resolution <133 eV). The accelerating voltage was set at 200 kV during the TEM measurement. The nanoparticle powders were cast on a lacey carbon grid.

UV-Visible absorption spectra were recorded by means a Varian Cary-5000 spectrometer, coupled with an integration sphere for diffuse reflectance acquisition, using a Carywin-UV/scan software. A sample of Teflon with 100% reflectance was employed as the reference. Spectra were registered in the 200–800 nm range at a scan rate of 240 nm/min with a step size of 1 nm. The measured reflectance intensities were

converted into absorbance with the Kubelka-Munk function. Then, the optical band gap energies were calculated considering that the energy dependence of the absorption coefficient (α) for semiconductors in the region near the absorption edge is given by

$$\alpha \propto \frac{(h\nu - E_{gap})^{\eta}}{h\nu}$$

where $h\nu$ is the energy of the incident photon and E_{gap} is the optical absorption energy. η depends on the type of optical transition and, in crystalline semiconductors, is 1/2 (direct-allowed), 3/2 (direct-forbidden), 2 (indirect-allowed), and 3 (indirect-forbidden). For what concerns ZnO and CeO_2, they show a direct-allowed optical transition, with a value of 1/2 for η. Finally, since the scattering coefficient weakly depends on energy and $F(R_\infty)$, it can be assumed as proportional to the absorption coefficient within the narrow range of energy containing the absorption edge feature.

$$F(R_\infty) = \frac{(h\nu - E_{gap})^{\eta}}{h\nu}$$

Then, the plot $(F(R_\infty)*h\nu)^{1/\eta}$ versus $h\nu$ can be used to determine the absorption edge energy (Tauc plot) method.

Electron paramagnetic resonance (EPR) measurements for the materials irradiated in vacuum and gas atmospheres were performed using a CW-EPR EMX-Bruker spectrometer operating at the X-band (9.5 GHz), equipped with a cylindrical cavity working at 100 kHz field modulation. The spectra were recorded at 77 K. All samples were treated under vacuum at 573 K for 30 minutes and subsequently oxidized in the presence of 50 mbar of molecular oxygen at 673 K for 2h. At the end of the treatment, the excess molecular oxygen was removed and the measurements were performed under vacuum or oxygen atmosphere. *In-situ* irradiation was performed, using a 1000 W xenon lamp (Oriel Instruments) equipped with an IR water filter, to which different band pass filters (Newport-20CGA, $\lambda \geq 400$ nm, $\lambda \geq 420$ nm, $\lambda \geq 455$ nm and $\lambda \geq 495$ nm) were applied.

The formation of •OH radical species upon irradiation at the solid-water interface was monitored by the EPR spin trapping technique using a Miniscope 100 spectrometer from Magnetech and using DMPO (5,5-dimethyl-1-pyrroline-N-oxide, Alexis Biochemicals, San Diego, CA) as spin trapping agent.

3. Results and discussion

Structural, morphological and optical characterization

Fig. 1 compares the diffraction patterns of both bare (panel A) and doped (panel B) ZnO materials prepared by different synthetic procedures. As first, it is possible to appreciate that all the difractograms in Panel A exhibits the pattern typical of the wurtzitic structure of zinc oxide; the Ce-containing mixed samples, in panel B, are characterized by the presence of a further very tiny and bare reflection, revealing the presence of the CeO_2 phase.

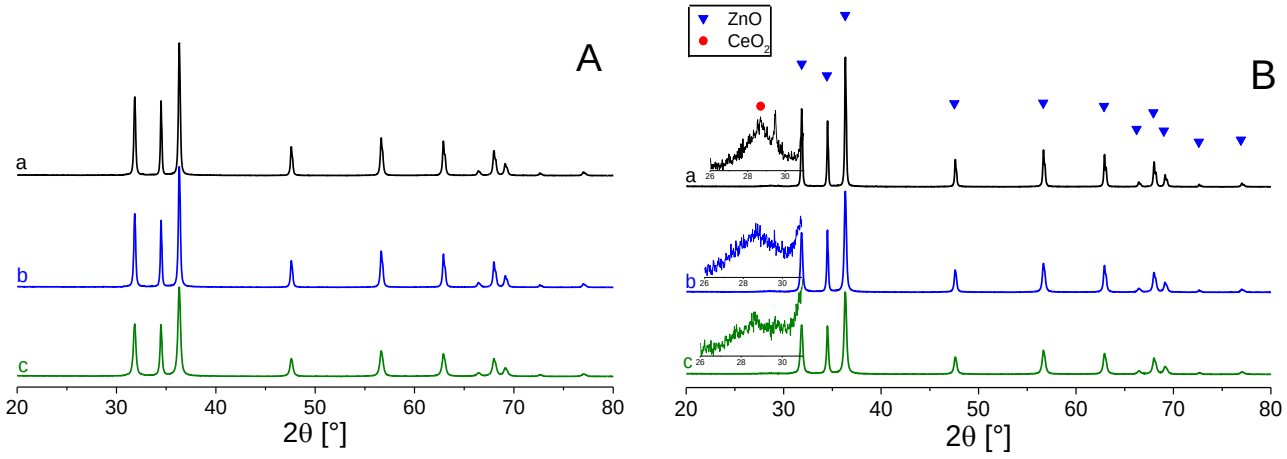

Figure 1. *XRD patterns of the synthetized materials. Panel A: a) ZnO-H, b) ZnO-HP1, c) ZnO-HP2. Panel B: a) CZ1-H, b) CZ1-HP1, c) CZ1-HP2. The red dot evidences the weak diffraction peak due to CeO_2.*

It is possible to note that all the sample patterns don't show any other reflections due to the presence of the template organic phase (P_{123}): this means that the calcination step has been effective in the elimination of the co-polymer. Comparing the pattern recorded for materials synthetized with Pluronic (b) and c) in both panels) with those of samples prepared without the template (ZnO-H, panel A and CZ1-H, panel B), it can be deduced that all the samples maintain a good degree of crystallinity, since their reflections appear still sharp and intense as in the case of ZnO-H and CZ1-H. Despite this, a little broadening and loss in intensity of the reflections occurs, as confirmed by Scherrer analysis and by the specific surface areas (BET method, see Table 1). For the material synthetized with the template agent it is possible to assert that they maintained a satisfying degree of crystallinity, despite a slight increasing of the specific surface area.

Sample	$d_{(XRD)}$ ZnO *(nm)*	$d_{(XRD)}$ CeO_2 *(nm)*	BET (m^2g^{-1})
ZnO-H	362 ± 7		< 10
CZ1-H	350 ± 11	17	<10
ZnO-HP1	71.1 ± 10.9		12
CZ1-HP1	50.1 ± 4.1	4	16
ZnO-HP2	39.2 ± 3.4		18
CZ1-HP2	38.7 ± 2.8	4	21

Table 1: *Crystallites size from Scherrer calculation performed on XRD patterns and BET surface area for the synthetized samples.*

The information still derivable from Table 1 is that the HP2 sample, prepared using a higher Pluronic amount show a smaller crystallite size and a higher surface area with respect to the ones synthetized with a lower polymer amount (HP1).

The morphological characterization of CZ1-HP1 and CZ1-HP2 materials performed by HRTEM reported in Fig. 2 evidence the formation of quasi-spherical particles of ZnO, characterized by hollows spheres, studded by very small particles of CeO_2.

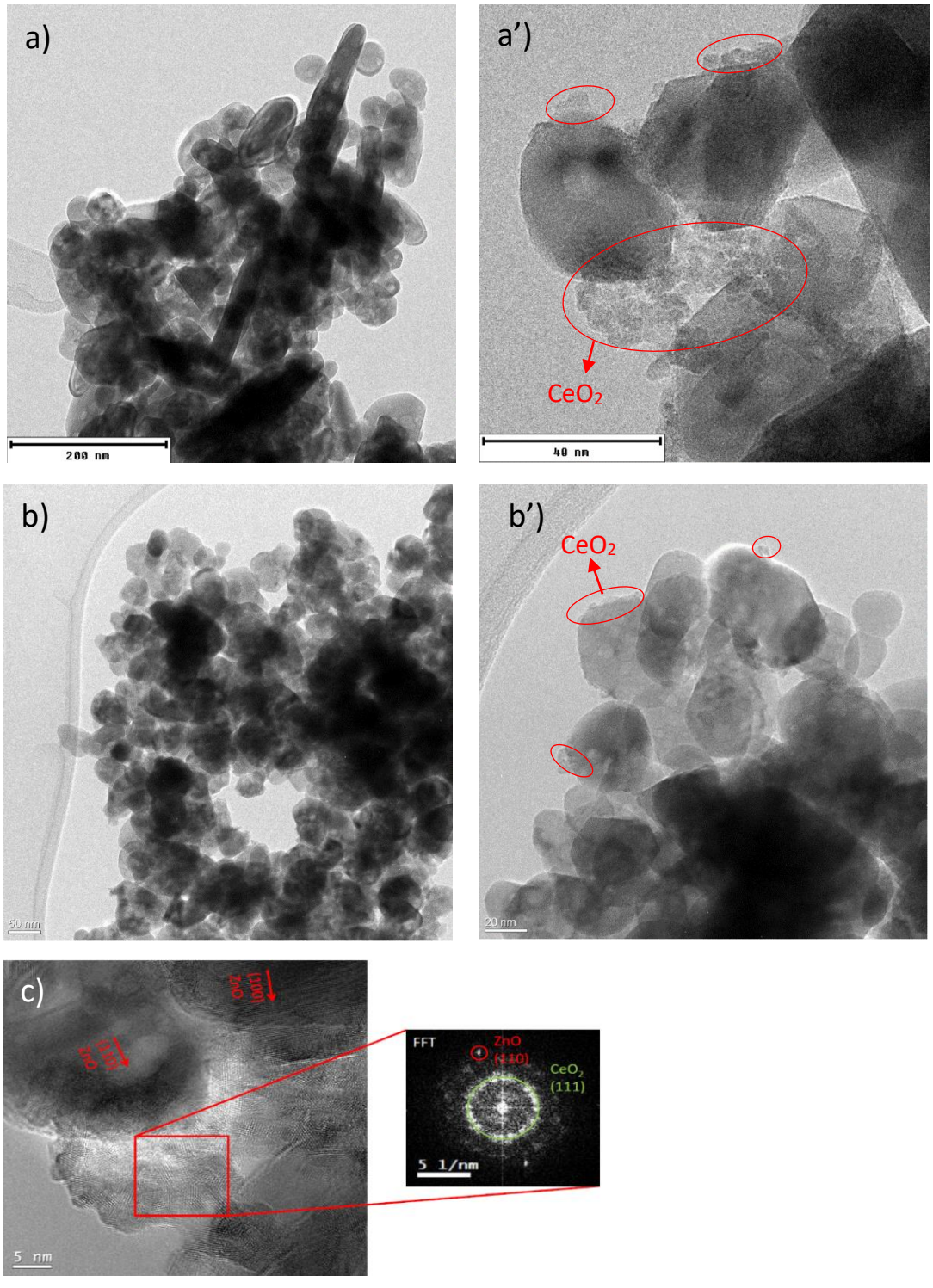

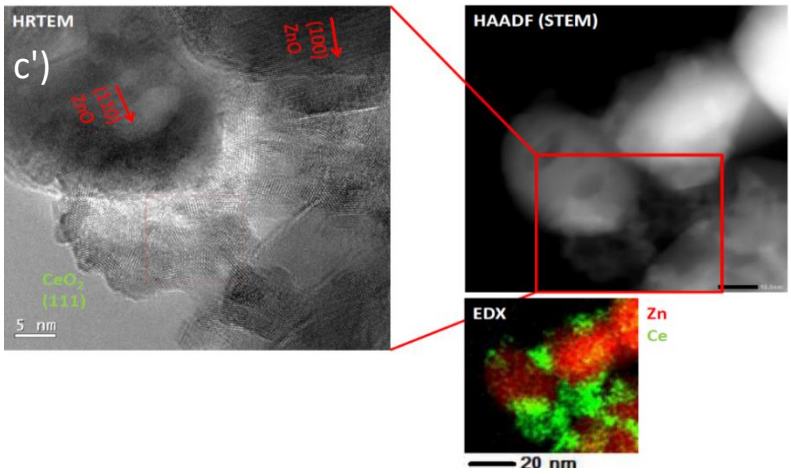

Figure 2. *TEM images of: a) CZ1-HP1, a') CZ1-HP1 enlargement, b) CZ1-HP2, b') CZ1-HP2 enlargement, c) High Resolution TEM (HR-TEM) image of CZ1-HP1. The structure was identified by a Fast Fourier Transformation (FFT) of the HR-TEM image as the CeO_2 phase and the surrounding matrix as the ZnO phase. c') EDS intensity maps of CZ1-HP1 (Ce = green, Zn = red).*

In the case of ZnO-H and CZ1-H [4, 17] the particles prepared in the absence of template appear very different in size and shape, mostly exhibiting a platelet shape. The hollow spheres obtained using the template represent an improving of the morphology since it has been already observed that this kind of structures increase the performance of a semiconducting metal-oxide based photocatalyst [3, 18-20]. The concentration of the templating agent influence the results. For CZ1-HP1 (Fig. 2, a) the morphology is still characterized by platelets accompanied by the appearance of small spherical particles (almost 50 nm), while for CZ1-HP2 (Fig. 2,b), synthetized with higher Pluronic concentration the particles size results more homogenous, with the hollow spheres that dominate the sample morphology. Moreover, in the case of CZ1-HP2 the ceria nanoparticles are more dispersed on the ZnO surface than in the case of CZ1-HP1, increasing the CeO_2-ZnO interfaces and then, possibly, the material activity.

The presence and identification of a ceria phase has been confirmed by the EDS maps (STEM technique); the results are shown in Fig. 2, c-c'). This measure certifies, as already mentioned elsewhere [21-24] that ceria is not incorporated into the ZnO lattice, but, rather, it form tiny particles, aggregated and stabilized on zinc oxide surface. It is also evident that ceria particles are well distributed and the interaction area between ceria and ZnO interfaces is quite extended.

The evaluation of the optical band gap has been performed by means UV-vis DR spectroscopy; the outcomes are plotted in Fig. 3.

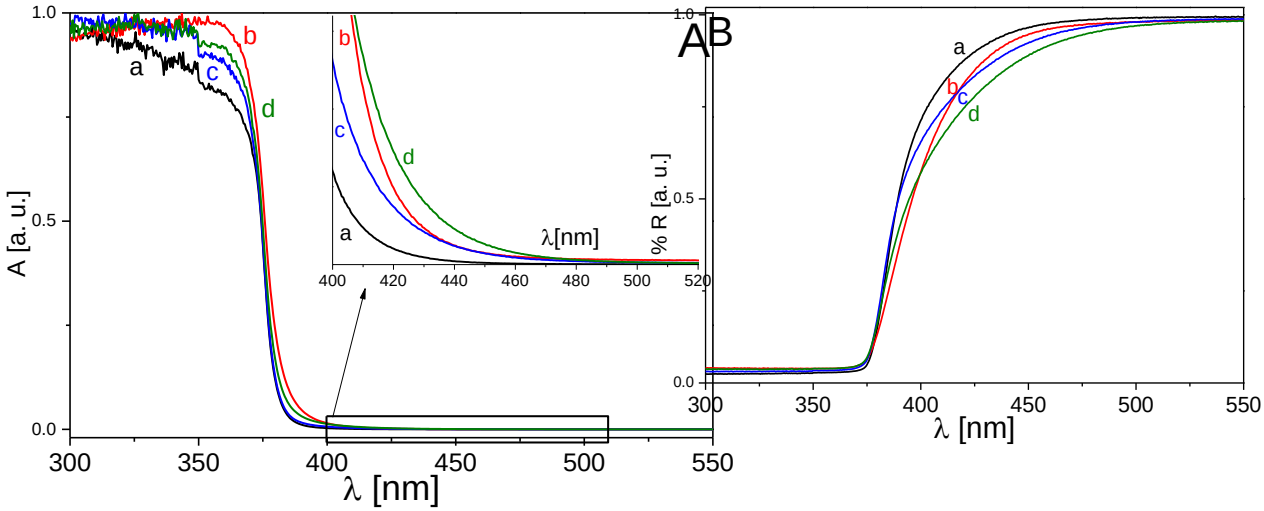

Figure 3. *Panel A: Absorbance Kubelka-Munk transformed diffuse reflectance spectra: a) ZnO-HP1, b) ZnO-HP2, c) CZ1-HP1 and d) CZ1-HP2. Panel B: Diffuse reflectance spectra.*

It can be noted that both bare and mixed samples show the valence band – conduction band transition typical of ZnO [25, 26], with a calculated E_g value around 3.3 eV for the four samples. However, having a look at the magnification in panel A, a contribution of the classic absorption trend of CeO_2 shows up in the case of the mixed samples (spectra c) and d)), further confirming the fact that Ce ions are not dispersed into the ZnO matrix, but rather, they form cerium dioxide particles decorating its surface[26-28]

EPR evidence of light-induced charge carriers formation and stabilization

The behaviour of the of the activated mixed samples CZ1-HP1 and CZ1-HP2 upon visible illumination at 77 K and in vacuum is described in Fig. 4 (panels A and B, respectively). A qualitative comparison of the EPR spectra obtained upon different illumination conditions highlights that both the mixed oxides are sensitive to visible wavelengths, with an improves absorption for the highest Pluronic amount employed during the synthesis. For sake of brevity, only the comparison between CZ1-HP1 and CZ1-HP2 will be reported, but it is worth to mentioning that also bare ZnO-HP1 and ZnO-HP2 show some unexpected photoactivity upon visible light irradiation, with the activity of ZnO-HP2 slightly higher than that ZnO-HP1.

In Fig. 4, panel A and B, the EPR spectra for CZ1-HP1 and CZ1-HP2, in dark (line a) and during irradiation of the samples kept under vacuum employing polychromatic light having different wavelengths, are reported. The spectra recorded in dark are not a flat line indicating the presence of a small amount of paramagnetic defects in the starting materials.

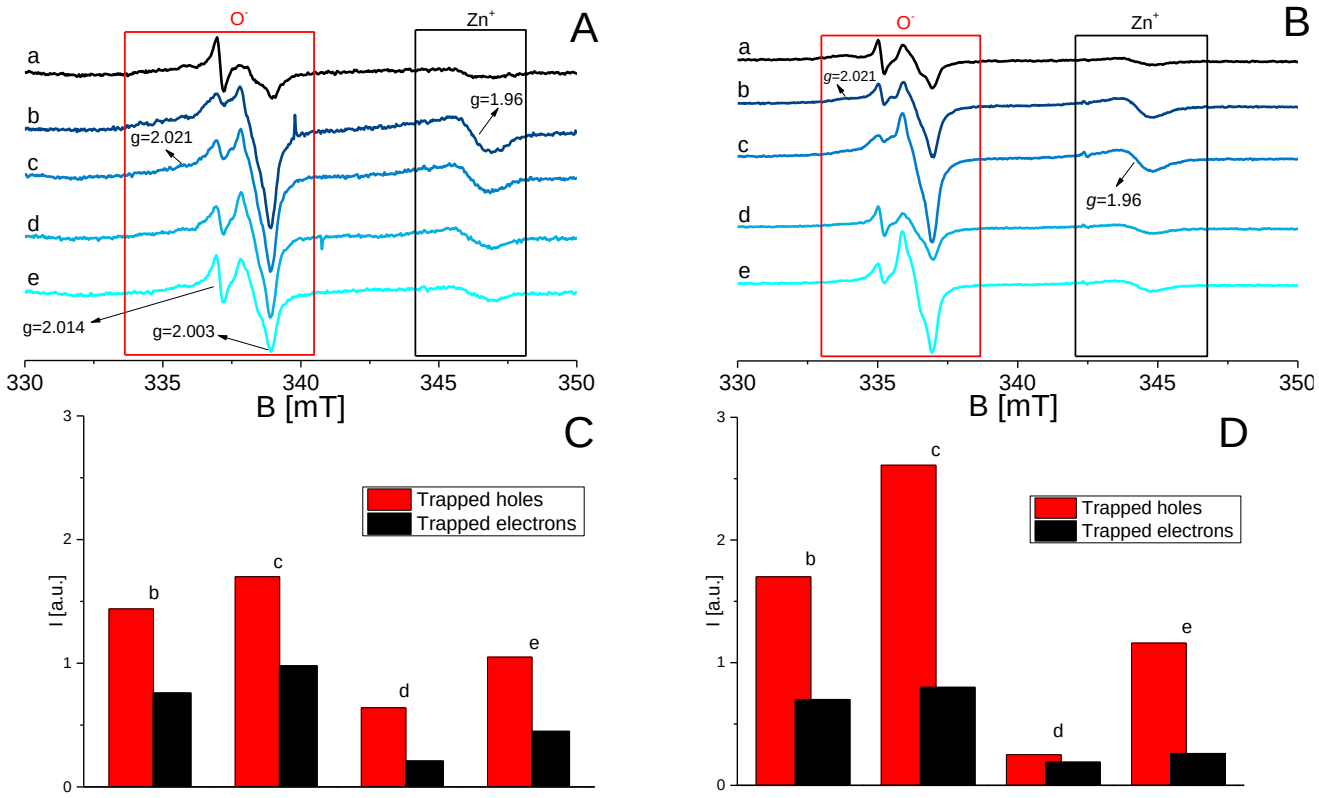

Figure 4. *Panel A: EPR spectra recorded under vacuum at 77K of (a) activated CZ1-HP1 (recorded in the dark), (b) upon irradiation with λ>400 nm, (c) λ>420nm, (d) λ>455nm and (e) λ>495nm. Panel B: EPR spectra recorded under vacuum at 77K of (a) activated CZ1-HP2 (recorded in the dark), (b) upon irradiation with λ>400 nm, (c) λ>420nm, (d) λ>455nm and (e) λ>495nm. Panel C and D: integrated intensities of the EPR signals (trapped holes and trapped electrons) as a function of the irradiation wavelength for CZ1-HP1 and CZ1-HP2, respectively. The intensity of the starting signal in a) (recorded in the dark) has been subtracted from the experimental values.*

A deeply assessment of the recorded EPR spectra allows determining that already before the irradiation procedures (Fig. 4, Panel A and B, a) the two materials shows some paramagnetic signals in two distinct regions of the magnetic field (x axis), respectively at lower and higher values than the free spin value (g_e = 2.0023), and attesting the highly defectivity nature of the matrix. The one at higher magnetic field is characterized by a quasi-isotropic line at g ~ 1.96 (black rectangle in Fig. 4, panels A and B) already reported in various EPR zinc oxide studies, whose assignation is still under debate. The most accepted attribution deals with the stabilization of an electron in shallow donor impurities such as Zn^+ ions.[27, 29-32] On the other hand, the complex signal at lower magnetic field aroused by the overlapping of two paramagnetic species:

the first undoubtedly attributed to O^- species in ZnO, characterized by an axial shape with $g_{\perp}$ = 2.021 and $g_{//}$ = 2.003 (red rectangle in Fig. 5, panels A and B),[33-35] and the second exhibiting an isotropic line at g = 2.014, ubiquitously present in ZnO materials and associated with the stabilization of the unpaired electron in intra-band gap defect states.[27, 36]

Generally, the irradiation (especially with UV light) of the ZnO matrix produces electro-hole pairs that can recombine or travel in the solid; when the irradiation is conducted at 77 K and in vacuum atmosphere (no surface charge transfer possible) the surviving charge carriers can be stabilized in the solid, namely the electrons in cation sites and the holes in the anion sites. Experimentally, this results in the growth of the symmetric line at g ~ 1.96 due to the trapping of photogenerated electrons as Zn^+ (1) and the simultaneous increase of the axial signal due to the trapping of photoinduced holes at the O^- sites.

$$e^-_{(CB)} + Zn^{2+} \rightarrow Zn^+ \qquad (1)$$

$$h^+_{(VB)} + O^{2-} \rightarrow O^- \qquad (2)$$

In Fig. 4, panels A and B it is possible to note a consistent increase of the EPR signals due to trapped electrons and holes upon visible irradiation, attesting the photoactivity nature of the prepared mixed systems; moreover, the material synthetized with a higher template content seems exhibiting higher charge carriers separation. In order to support this thesis, we performed the double integration of the EPR spectra (before and after irradiation) for the trapped electrons (Zn^+) and holes (O^-) signals. In addition, we normalized the intensity as a function of the different irradiation wavelengths and subtracting the spectrum intensity of the no-irradiated materials (spectrum a) in Fig. 4, panel A and B), thus highlighting the actual charge carriers separation for the two samples that can become comparable, as reported in Fig. 4, panel C and D. It comes out that CZ1-HP2 shows a slightly higher electron-hole pairs promotion upon the different wavelengths irradiation respect CZ1-HP1, testifying that an optimum Pluronic amount during the synthetic route might effectively generate a greater homogeneity of the hallow spheres morphology and a better dispersion of ceria on ZnO; this would guarantee and increased presence of CeO_2-ZnO intimate connections, an indispensable condition for the employment of the mixed system as a visible light active photocatalyst.

Still focusing the attention on Panel C and D of Fig. 4, we can attest that for both CZ1-HP1 and CZ1-HP2 the best charge carriers separation was registered for $\lambda \geq 420$ nm, while an abrupt decrease of the intensity was observed for $\lambda \geq 455$ nm: this last experimental evidence could be explained considering that at this particular wavelength irradiation the photoexcited electrons from the ZnO valence band can be selectively trapped in intrinsic defects establishing intra-band gap states, as reported in previous works.[27, 37-41]Finally, as reported in our previous work, [22] the amount of photogenerated holes is higher with respect to that of trapped electrons (*g* = 1.96). This fact has been explained considering that at the CeO_2-ZnO interfaces the main fraction of photogenerated electrons are not stabilized on ZnO (conduction band electrons or shallow donors) but are transferred to Ce *4f* level, reducing Ce^{4+} to Ce^{3+}. Ce^{3+} is a paramagnetic ion but its signal is

undetectable in the experimental conditions of this work [22]. For this reason, a fraction of the photogenerated electrons is not detected in the experiment. The efficient charge separation observed (Fig. 4) firmly confirms that CeO_2-ZnO mixed materials are rather sensitive to visible light. The charge separation ability of UV light (line b in Panels A and B) is surprisingly lower than that of visible frequencies.

In Fig. 5 the EPR spectra of CZ1-HP1 and CZ1-HP2 upon irradiation with band pass filter at 420 nm are compared. It is evident that the second sample shows higher charge carriers separation ability upon visible light illumination: this could be attributed to the fact that the higher P_{123} content gives rise to smaller and more defined hollow spheres, characterized by higher homogeneity and a better dispersion of the ceria nanoparticles on ZnO surface, generating more photo-sensitive interfaces.

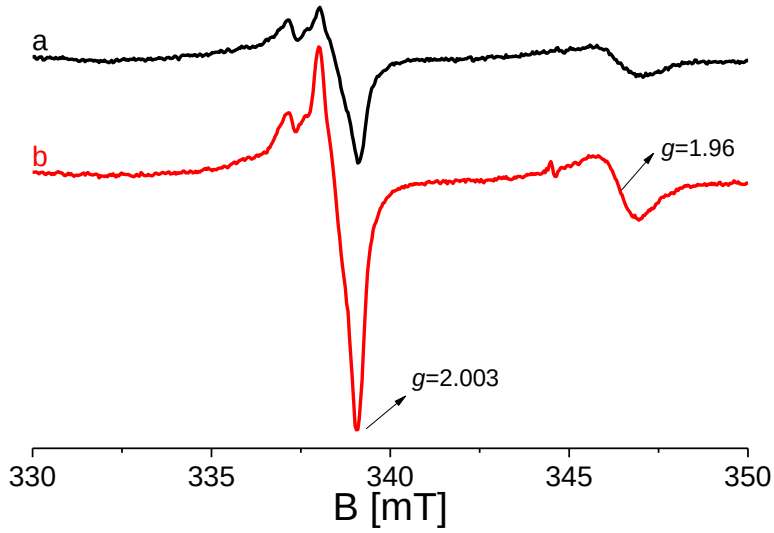

Figure 5. *EPR spectra recorded under vacuum at 77K of (a) CZ1-HP1 and (b) CZ1-HP2 upon irradiation with λ>420nm.*

EPR spectroscopy upon irradiation under reactive oxygen atmosphere and in water.

The promising results obtained for the samples CZ1-HP1 and CZ1-HP2 irradiated under polychromatic visible light (λ>420 nm) in vacuum conditions led us to perform the same experiment in the presence of oxygen atmosphere. It has been already outlined elsewhere [47, 48] that oxygen is a strong electron scavenger: we were therefore interested to investigate if the electrons produced by visible irradiation were able to migrate to the surface of the mixed oxides and react with oxygen, generating the paramagnetic, and then EPR detectable, superoxide species (O_2^-). The experiment outcomes are presented in Fig. 6 for CZ1-HP1 and CZ1-HP2 in panel A and B, respectively.

In the case of CZ1-HP1 (panel A) the formation of O_2^- is monitored in terms of the change of the complex signals at higher *g* values (left side of the spectrum) with respect to the signal after irradiation in vacuum atmosphere. The formation of superoxide species is even more evident for the sample CZ1-HP2 (panel B) where the typical signal of O_2^- chemisorbed on Zn^{2+} (g_{zz}=2.050-2.055, g_{yy}=2.009 and g_{xx}=2.003 [36, 47, 49, 50])

and on Ce^{4+} ($g_{zz} = g_{//} = 2.032$ and $g_{yy} = g_{zz} = g_{\perp} = 2.011$ [51]) can be easily recognized. In agreement with previous findings, it comes out that the CeO_2-Zno sample synthetized using a higher template concentration is more efficient in the surface electron transfer to O_2 induced by purely visible light.

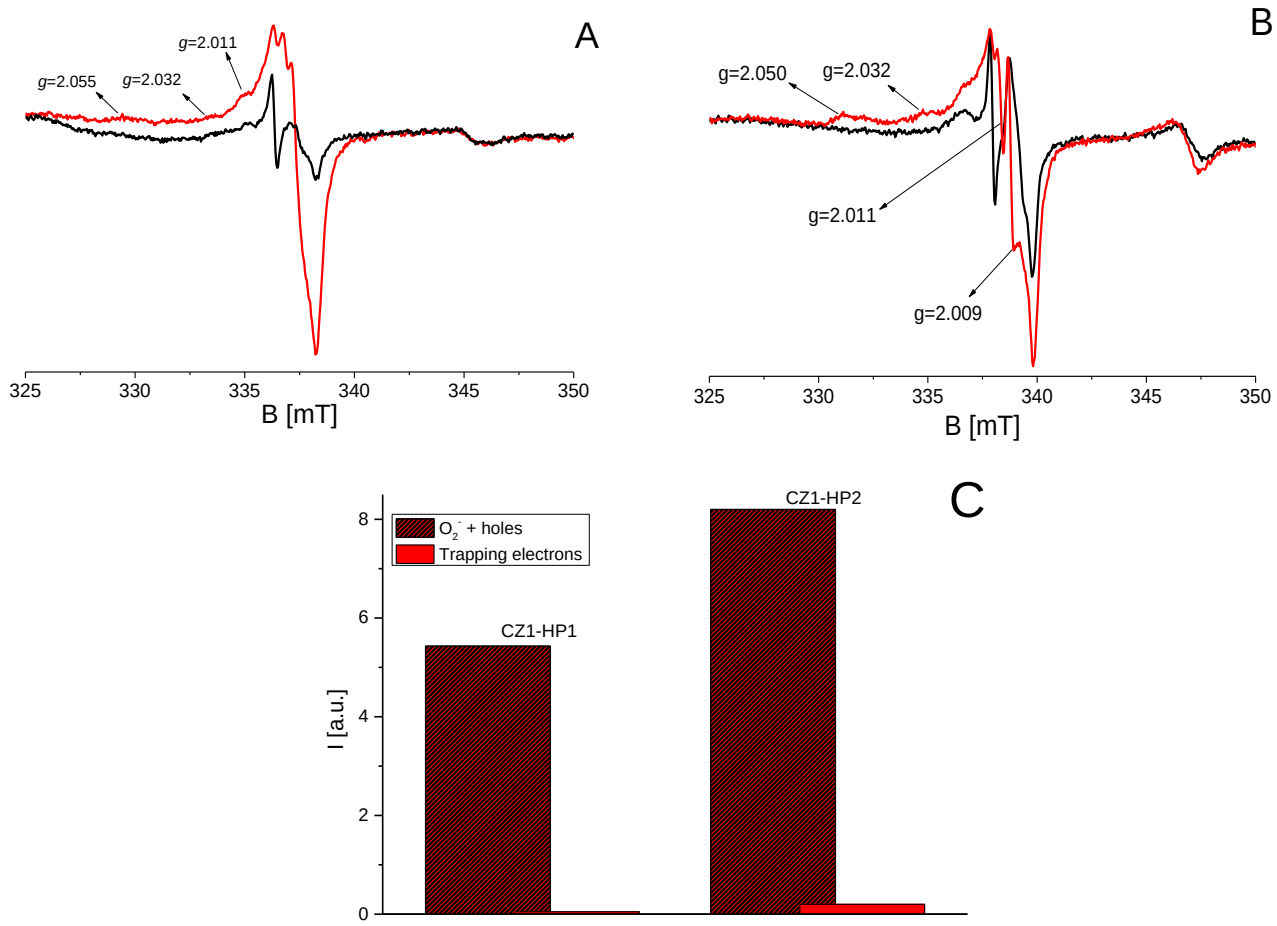

Figure 6. *Panel A: EPR spectra at 77 K of activated CZ1-HP1 (black line) and irradiation with visible light (λ> 420 nm) in presence of molecular oxygen (red line). Panel (B): EPR spectra at 77 K of activated CZ1-HP2 (black line) and irradiation with visible light (λ> 420 nm) in presence of molecular oxygen (red line). Panel C: Integrated intensities of the EPR spectra upon irradiation in oxygen using λ > 420 nm for CZ1-HP1 and CZ1-HP2, respectively.*

As in the case of irradiation under vacuum (Fig. 4-5), it seems that the superior morphology of the CZ1-HP2 sample, together with its higher surface area, is the reason of the higher photoactivity with respect to the CZ1-HP1 one, as reported by the histogram in Fig. 6 panel C.

The irradiation of the samples generates two different charges: electrons and holes. As described above electrons are scavenged by molecular oxygen. To detect holes and in particular to verify the hole activity at the solid-liquid interface we irradiated an aqueous suspension of the materials with visible light having λ>420 nm, in presence of DMPO (5,5-dymethil-1-pyrroline-N-oxide) that acts as spin trapping agent for hydroxyl

radicals (•OH) in solution forming a stable radical adduct (DMPO/ •OH) easily monitored by EPR spectroscopy [52]. As it is well known[53, 54], •OH radicals are the most powerful oxidative species that can be formed in solution and their production upon illumination is of crucial importance in photo-degradation processes.

The process is described by the following equation (3):

$$h^{+}_{(VB)} + H_2O \rightarrow OH^{\bullet} + H^{+} \qquad (3)$$

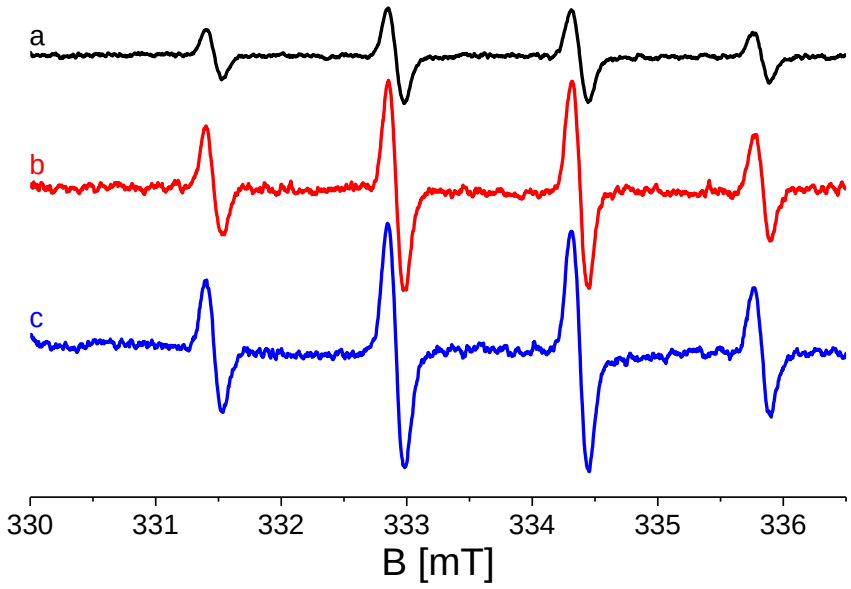

Figure 7. *EPR spectra of the DMPO/•OH adduct produced by irradiation with λ≥420 nm of an aqueous suspensions of (a) CZ1-H, (b) CZ1-HP1 and c) CZ1-HP2 (after 30' of irradiation).*

Fig. 7 reveals that the sample CZ1-HP2 produces the highest amount of OH• radicals when irradiated with λ > 420 nm. Also for CZ1-HP1 the production is appreciable and higher than in the case of CZ1-H (no template, platelets morphology). The improved quality brought about by the hollow spheres morphology, the higher dispersion of CeO_2 on ZnO (with, consequently, a higher extension of the heterojunction between the two phases) and, finally, the larger surface area can explain the superior photoactivity of the materials here described. These are, as already outlined, most promising VLA systems in photocatalytic application since they show sensitivity to an extended range of visible wavelengths.

4. Conclusions

In this paper the study of a strategy to improve the photocatalytic activity of the already very well established CeO_2-ZnO VLA photocatalyst has been described. In particular, the enhancement of the photo activity has been achieved by means of the modification of the material morphology. In order to set this, two different amounts of Pluronic, acting as template agent, have been used in the synthesis obtaining a hollow spheres particles morphology that is better defined in the case of the higher template concentration.

Morphological set up, crystallinity and specific surface area have been investigated and it has been revealed that the modified materials, in parallel with the maintenance of a good crystallinity, show a higher surface area and the desired hollow spheres morphology, that is important in the field of photocatalytic applications. Moreover, EPR analysis has revealed that the mixed system synthetized with higher co-polymer content is more efficient in the generation of electron-hole pairs upon visible irradiation and that these photogenerated charge carriers are able to reach the solid and react with the surrounding environment (as shown by irradiation in oxygen atmosphere and by the spin trapping in solution). Concluding, the hollow spheres morphology achieved through the synthesis here reported leads to systems with a higher photoactivity under visible irradiation than the same system displaying the classic platelets morphology. Although the experimental parameters (reactants and template concentrations, calcination temperature and time) have to be still optimized, this work states the basis for a remarkable improvement of the already tested CeO_2-ZnO heterojunction, active in the abatement of classical and emerging organic pollutants using visible light.

References

[1] A.B. Djurisic, Y.L. Leung, A.M.C. Ng, Strategies for Improving the Efficiency of Semiconductor Metal Oxide Photocatalysis, Mater. Horiz 1 (2014) 400-410.
[2] K.M. Lee, C.W. Lai, K.S. Ngai, J.C. Juan, Recent Developments of Zinc Oxide Based Photocatalyst in Water Treatment Technology: a Review, Water Res 88 (2016) 428-448.
[3] J. Kegel, I.M. Povey, M.E. Pemble, Zinc Oxide for Solar Water Splitting: a Brief Review of the Material's Challenges and Associated Opportunities, Nano Energy 54 (2018) 409-428.
[4] M.C. Paganini, D. Dalmasso, C. Gionco, V. Polliotto, L. Mantilleri, P. Calza, Beyond TiO_2: Cerium-Doped Zinc Oxide as a New Photocatalyst for the Photodegradation of Persistent Pollutants, ChemistrySelect 1 (2016) 3377-3383.
[5] P. Calza, C. Gionco, M. Giletta, M. Kalaboka, V.A. Sakkas, T. Albanis, M.C. Paganini, Assessment of the Abatement of Acelsulfame K Using Cerium Doped ZnO as Photocatalyst, J. Hazard. Mater. 323 (2016) 471-477.
[6] N.C. Birben, M.C. Paganini, P. Calza, M. Bekbolet, Photocatalytic Degradation of Humic Acid using a Novel Photocatalyst: Ce-doped ZnO, Photochem. Photobiol. Sci. (2016) 24-30.
[7] O. Bechambi, A. Touati, S. Sayadi, W. Najjar, Effect of Cerium Doping on the Textural, Structural and Optical Properties of Zinc Oxide: Role of Cerium and Hydrogen Peroxide to Enhance the Photocatalytic Degradation of Endocrine Disrupting Compounds, Mater. Sci. Semicond. Process. 39 (2015) 807-816.
[8] O. Bechambi, L. Jlaiel, W. Najjar, S. Sayadi, Photocatalytic Degradation of Bisphenol A in the Presence of Ce-ZnO: Evolution of Kinetics, Toxicity and Photodegradation Mechanism, Mater. Chem. Phys. 173 (2016) 95-105.
[9] M.A.M. Ahmed, W.E. Meyer, J.M. Nel, Structural, Optical and Electrical Properties of a Schottky Diode Fabricated on Ce doped ZnO Nanorods Grown using a Two Step Chemical Bath Deposition, Mater. Sci. Semicond. Process. 87 (2018) 187-194.
[10] Z. Xu, Q. Hou, F. Guo, X. Jia, C. Li, W. Li, Effects of Strain on the Optical and Magnetic Properties of Ce-doped ZnO, Curr. App. Phys. 18 (2018) 1465-1472.
[11] J.C. Sin, S.M. Lamb, K.T. Leec, A.R. Mohamed, Preparation of Cerium-Doped ZnO Hierarchical Micro/Nanospheres with Enhanced Photocatalytic Performance for Phenol Degradation under Visible Light, J. Mol. Catal. A: Chem. 409 (2015) 1-10.
[12] R. Manimozhi, D. Ranjith Kumar, A.P. Gnana Prakash, Enhanced Solar Light Driven Photocatalytic Degradation of Organic Dye Using Solution Combustion Synthesized CeO_2-ZnO Nanocomposites, J. Electron. Mater. 47 (2018) 6716-6721.
[13] K. Negi, M. Kumar, M.S. Chauhan, Solution Combustion Synthesis of CeO2/ZnO Nano-Composite as a Potential Scaffold for Detection and Degradation of P-Nitrophenol, Mater. Chem. Phys. 226 (2019) 59-65.
[14] C. Wang, H. Fan, X. Ren, J. Fang, Room Temperature Synthesis and Enhanced Photocatalytic Property of CeO_2/ZnO Heterostructures, Appl. Phys. A 124 (2018).
[15] E. Wuilloud, B. Delley, D. Schneider, Y. Baer, Spectroscopic Evidence for Localized and Extended f-Symmetry States in CeO_2, Phys. Rev. Lett. 53 (1984) 202-205.
[16] J. Jiang, K. Zhang, X. Chen, F. Zhao, T. Xie, D. Wang, Y. Lin, Porous Ce-doped ZnO Hollow Sphere with Enhanced Photodegradation Activity for Artificial Waste Water, J. Alloys Compd. 699 (2017) 907-913.
[17] E. Cerrato, C. Gionco, I. Berruti, F. Sordello, P. Calza, M.C. Paganini, Rare earth ions doped ZnO: Synthesis, characterization and preliminary photoactivity assessment, J. Solid State Chem. 264 (2018) 42-47.
[18] P. Pichat, Photocatalysis and Water Purification: from Foundamentals to Recente Apllications, Weinheim, 2013.
[19] M. Li, Y. Liu, L. Dong, C. Shen, F. Li, M. Huang, C. Ma, B. Yang, X. An, W. Sand, Recent Advances on Photocatalytic Fuel Cell for Environmental Applications-The marriage of Photocatalysis and Fuel Cells, Sci. Total Environ. 668 (2019) 966-978.
[20] X. He, C. Zhang, Recent Advances in Structure Design for Enhancing Photocatalysis, J. Mater. Sci. 54 (2019) 8831-8851.
[21] E. Cerrato, C. Gionco, M.C. Paganini, E. Giamello, Photoactivity Properties of ZnO Doped with Cerium Ions: an EPR Study, J. Phys. Condens. Matter. 29 (2017) 1-7.

[22] E. Cerrato, C. Gionco, M.C. Paganini, E. Giamello, E. Albanese, G. Pacchioni, Origin of Visible Light Photoactivity of the CeO_2/ZnO Heterojunction, ACS Appl. Energy Mat. 1 (2018) 4247-4260.
[23] P. Caregnato, K.R. Espinosa Jiménez, P.I. Villabrille, Ce-doped ZnO as Photocatalyst for Carbamazepine Degradation, Catal. Today 372 (2021) 183-190.
[24] M. Rezaei, A. Habibi-Yangjeh, Microwave-Assisted Preparation of Ce-doped ZnO Nanostructures as an Efficient Photocatalyst, Mater. Lett. 110 (2013) 53-56.
[25] U. Özgür, Y.I. Alivov, C. Liu, A. Teke, M.A. Reshchikov, S. Doğan, V. Avrutin, S.J. Cho, H. Morkoç, A Comprehensive Review of ZnO Materials and Devices, J. Appl. Phys. 98 (2005) 041301-041301103.
[26] A. Mang, K. Reimann, S. Rubenacke, Band Gaps, Crystald-Field Splitting, Spin-Orbit Coupling, and Exciton Binding Energies in ZnO under Hydrostatic Pressure, Solid State Commun. 94 (1995) 251-254.
[27] E. Cerrato, M.C. Paganini, E. Giamello, Photoactivity under Visible Light of Defective ZnO Investigated by EPR Spectroscopy and Photoluminescence, J. Photochem. Photobiol., A 397 (2020) 112531.
[28] A. Janotti, C.G. Van de Walle, New insights into the role of native point defects in ZnO, J. Cryst. Growth 287 (2006) 58-65.
[29] D.C. Look, J.W. Hemsky, Residual Native Shallow Donor in ZnO, Phys. Rev. Lett. 82 (1999) 2552-2555.
[30] P.H. Kasai, Electron Spin Resonance Studies of Donors and Acceptors in ZnO, Phys. Rev. 130 (1963) 989-995.
[31] L.E. Halliburton, N.C. Giles, N.Y. Garces, M. Luo, C. Xu, L.B.A. Boatner, Production of Native Donors in ZnO by Annealing at High Temperature in Zn Vapour, Appl. Phys. Lett. 87 (2005) 1721081-1721083.
[32] D.M. Hofmann, A. Hofstaetter, F. Leiter, H. Zhou, F. Henecker, B.K. Meyer, S.B. Orlinskii, J. Schmidt, P.G. Baranov, Hydrogen: a Relevant Shallow Donor in Zinc Oxide, Phys. Rev. Lett. 88 (2002) 0455041-0455044.
[33] A.M. Volodin, S.E. Malykhin, G.M. Zhidomirov, O^- Radical Anions on Oxide Catalysts: Formation, Properties, and Reactions, Kinet. Catal. 52 (2011) 605-619.
[34] M. Che, A.J. Tench, Characterization and Reactivity of Mononuclear Oxygen Species on Oxide Surfaces, Adv. Cat. 31 (1982).
[35] N.B. Wong, Y.B. Taarit, J.H. Lunsford, Formation of O^- in ZnO from the Dissociation of Adsorbed N_2O, J. Chem. Phys. 60 (1974) 2148-2151.
[36] J.H. Lunsford, J.P. Jayne, Electron Paramagnetic Resonance of Oxygen on ZnO and Ultraviolet Irradiated MgO J. Chem. Phys. 44 (1966) 1487-1492.
[37] A. Poppl, G. Volkel, ESR and Photo-ESR Investigations of Zinc Vacancies and Interstitial Oxygen Ions in Undoped ZnO Ceramics, Phys Stat. Sol. A 125 (1991) 571-581.
[38] A. Poppl, G. Volkel, ESR and Photo-ESR Investigations of the Vl Centre in ZnO Raw Material and Li-Doped ZnO Ceramic Powder, Phys. Stat. Sol. A 121 (1990) 1995-1204.
[39] G. Volkel, A. Poppl, B. Voigtsberg, Investigation of the Oxygen Vacancy Balance in ZnO Ceramics by Means of EPR, Phys. Stat. Sol. (a) 109 (1988) 295-299.
[40] S.M. Evans, N.C. Giles, L.E. Halliburton, L.A. Kappers, Further characterization of oxygen vacancies and zinc vacancies in electron-irradiated ZnO, Journal of Applied Physics 103 (2008) 043710.
[41] L.A. Kappers, O.R. Gilliam, S.M. Evans, L.E. Halliburton, N.C. Giles, EPR and optical study of oxygen and zinc vacancies in electron-irradiated ZnO, Nuclear Instruments and Methods in Physics Research Section B: Beam Interactions with Materials and Atoms 266 (2008) 2953-2957.
[42] N.Y. Garces, N.C. Giles, L.E. Halliburton, G. Cantwell, D.B. Eason, D.C. Reynolds, D.C. Look, Production of Nitrogen Acceptors in ZnO by Thermal Annealing, Appl. Phys. Lett. 80 (2002) 1334-1336.
[43] K.A. Muller, J. Schneider, Conduction Electron Spin Resonance in Group II-VI Semiconductors and Phosphors, Phys. Lett. 4 (1963) 288-291.
[44] D.G. Thomas, J.J. Lander, Hydrogen as a Donor in Zinc Oxide, J. Chem. Phys. 25 (1956) 1136-1142.
[45] C.G.V.d. Walle, Hydrogen as a Cause of Doping in Zinc Oxide, Phys. Rev. Lett. 85 (2000) 1012-1015.
[46] L.S. Vlasenko, Point defects in ZnO: Electron paramagnetic resonance study, Physica B: Condensed Matter 404 (2009) 4774-4778.
[47] M. Che, A.J. Tench, Characterization and Reactivity of Molecular Oxygen Species on Oxide Surfaces Adv. Catal. 32 (1983) 1-148.
[48] V. Polliotto, S. Livraghi, E. Giamello, Electron Magnetic Resonance as a Tool to Monitor Charge Separation and Reactivity in Photocatalytic Materials, Res. Chem. Intermed. 44 (2018) 3905-3921.

[49] M. Iwamoto, Y. Yoda, N. Yamazoe, T. Seiyama, Study of Metal Oxide Catalysts by Temperature Programmed Desorption. Oxygen Adsorption on Various Metal Oxides, J. Phys. Chem. 82 (1978) 2564-2570.
[50] K.-i. Tanaka, G. Blyholder, Adsorbed Oxygen Species on Zinc Oxide in the Dark and under Illumination, The Journal of Phg&al Chemistry 76 (1972) 3184-3187.
[51] M. Che, J.F.J. Kibblewhite, A.J. Tench, M. Dufaux, C. Naccache, Oxygen Species Adsorbed on CeO_2/SiO_2 Supported Catalysts, J. Chem. Soc., Faraday Trans. 1 69 (1973) 857-863.
[52] D. Dvoranová, V. Brezová, M. Mazúr, M.A. Malati, Investigations of Metal-Doped Titanium Dioxide Photocatalysts Appl. Catal. B 37 (2002) 91-105.
[53] N. Azbar, T. Yonar, K. Kestioglu, Comparison of Various Advanced Oxidation Processes and Chemical Treatment Methods for COD and Color Removal from a Polyester and Acetate Fiber Dyeing Effluent, Chemosphere 55 (2004) 35-43.
[54] K.E. O'Shea, D.D. Dionysiou, Advanced Oxidation Processes for Water Treatment, J. Phys. Chem. Lett. 3 (2012) 2112-2113.